Odderon as a Regge spin-3 oddball in pp and $p\bar{p}$ elastic scattering

Jingle B. Magallanes,[1,†] Prin Sawasdipol,[2,‡] Chakrit Pongkitivanichkul,[2,§] and Daris Samart[2,*]

[1]*Department of Physics, Mindanao State University—Iligan Institute of Technology, Iligan City, 9200, Philippines*

[2]*Khon Kaen Particle Physics and Cosmology Theory Group (KKPaCT), Department of Physics, Faculty of Science, Khon Kaen University, 123 Mitraphap Road, Khon Kaen, 40002, Thailand*

(Received 11 September 2023; accepted 11 January 2024; published 6 February 2024)

In this work, we propose that the odderon is a Regge spin-3 odd-glueball tensor. To demonstrate the proposal, we study the pp and $p\bar{p}$ elastic scattering by including the contributions of the spin-3 odderon and spin-2 pomeron exchange in the processes. The phenomenological effective Lagrangian approach is used to calculate the pp and $p\bar{p}$ elastic scattering amplitudes at the tree level. Additionally, the Donnachie-Landschoff ansatz of the odderon and pomeron propagators was used in further analysis. We fit the theoretical results with the various experimental data of the pp and $p\bar{p}$ scattering at the TeV scale to determine the model parameters in the present work. By using the model parameters, the Chew-Frautschi plot of the tensor odderon Regge trajectory is evaluated. As a result, the odderon spin-3 mass is predicted to be 3.2 GeV. In addition, a phase rotation is applied to the amplitude of our model in order to satisfy the geometric scaling at a very low t region. Moreover, the total cross section of our model is compatible with the results from TOTEM and its extrapolation from D0 collaboration. It was found that the total cross section also satisfies the Friossart bound at the Regge limit.

DOI: 10.1103/PhysRevD.109.034007

I. INTRODUCTION

Quantum chromodynamics (QCD) is a modern theory of strong interactions based on non-Abelian color SU(3) quantum gauge field theory describing the interaction of quarks and gluons. QCD is highly successful in explaining hadronic structures and interactions at high energies (momentum exchange) where the strong coupling is small and perturbative quantum field theory is applied. However, at a low energy regime, QCD is a strongly coupled theory that we cannot use the standard perturbative theory. On the other hand, hadron-hadron scattering in high center of mass energy ($\sqrt{s}$) but low momentum exchange (t) known as soft-high energy regime or a Regge limit of $s \to \infty$ and $s \gg t$, the perturbative QCD is also inapplicable. Before the birth of QCD, Regge theory is invented to describe the hadron-hadron collisions by using analytical properties of the scattering amplitudes [1] including a consideration of the complex angular momentum [2]. In the Regge theory, the amplitudes of the hadronic processes are scaled as s^J where J is the spin of the exchange particles called Reggeons with fixed relevant quantum numbers [3]. One can write down the spin as a linear function of t as $J = \alpha(t)$ in the complex angular momentum plane and the linear function $\alpha(t) = \alpha_0 + \alpha' t$ is called a Regge trajectory. In addition, the poles (Regge poles) correspond to the families of the exchange particles with increasing spins along the trajectories. As a result, the amplitudes of Regge theory are represented in terms of a sum over all possible exchange particles lying on the Regge trajectory. The cross sections of various hadronic processes in the soft-high energy scattering limit are successfully described by the Regge theory [4–7].

According to the experimental data of hadron-hadron scattering in the Regge limit, the total cross sections slowly grew up with the increase of s whereas the Regge trajectories of all known mesons are not sufficient to explain the experimental data. Then, a so-called pomeron was introduced to address this problem [8,9]. The pomeron is a Reggeon carrying all even charge transformations, vacuum quantum number, with the intercept of Regge trajectory $\alpha_0 \approx 1$. This yields the slow growth of the total cross section at large s [10,11]. Various approaches are trying to extract the information of the pomeron trajectory. The typical values of the parameters of the pomeron trajectory

*Corresponding author: darisa@kku.ac.th
†jingle.magallanes@g.msuiit.edu.ph
‡p.namwongsa@kkumail.com
§chakpo@kku.ac.th

from [12–14] are $\alpha_0 \approx 1.06$–1.08 and $\alpha' \approx 0.025$ GeV^{-2} [12–14]. The pomeron is generally considered as a bound state of the gluons (glueball). On the other hand, the odd charge-conjugation counterpart of the pomeron called odderon has been proposed by Ref. [15]. Similar to the pomeron, the odderon is considered as the glueball with the odd number of gluon compositions. The odderon might cause the different observables between pp and $p\bar{p}$ due to its charge-conjugation property, which is compatible with the experiment. However, the nature and properties of the pomeron and odderon are still unclear so far. A number of approaches have been used to calculate the properties (mass, spin, Regge trajectory etc.) of pomeron and odderon as glueballs [16–47]. A study of pomeron and odderon exchanges in pp and $p\bar{p}$ elastic scatterings in the soft-high energy regime has been extensively investigated in various frameworks for instances, phenomenological approaches [48–60], QCD inspired models [61–69], holographic QCD or AdS/CFT correspondence [70–79].

Recently, however, TOTEM and D0 collaborations have confirmed the existence of the odderon by comparing the experimental data between pp (extrapolated from previous several data) and $p\bar{p}$ at 1.96 TeV [80,81]. This reveals the contributions of the odderon in t-channel elastic scattering. After the TOTEM and D0 collaborations claimed the discovery of the odderon, several works were done to investigate the properties and scattering processes of the odderon [82–91].

Based on the discovery of the odderon and the relevant literature on the field theoretical framework in Ref. [48], we propose the odderon as a spin-3 tensor odd-glueball within the standard field theoretical framework. We study its consequences in pp and $p\bar{p}$ elastic scatterings. According to a constituent quark model, the odderon is composed of a three-gluon, and the lightest trajectory of the odderon is the spin-3, not the spin-1. This is because the odderon begins with a $J^{PC} = 3^{--}$ three-gluon $L = 0$ state with a maximum spin of 3. Similarly, the two-gluon bound state or pomeron starts with the s wave, and the spin and PC quantum number are assigned as $J^{PC} = 2^{++}$ glueball. Furthermore, a combined lattice QCD calculation and field theoretical Coulomb gauge QCD model confirmed that the odderon can be the oddball starting its Regge trajectory with $J^{PC} = 3^{--}$ [46]. Various theoretical approaches have also shown that the pomeron is likely to be the spin-2 tensor glueball instead of the scalar one [48,49,52,53,63,68,70,73–76]. Then the lowest tensor odderon in its Regge trajectory is spin-3 as explained previously. However, the slope, intercept, and mass of the odderon are not well understood.

In this work, we investigate the elastic scattering of pp and $p\bar{p}$ with the contributions of the odderon spin-3. The effective Lagrangian of the spin-3 odderon with protons is constructed by using a similar approach in Ref. [48]. Especially, a so-called Donnachie-Landschoff ansatz is used to represent the odderon and pomeron propagators. The contributions of the spin-2 pomeron exchange are also included in the calculation where the effective Lagrangian of pomeron and protons is taken from Ref. [48]. Then the differential cross sections of the pp and $p\bar{p}$ elastic scattering are calculated. After a careful statistical analysis, we fit the parameters of our model with several relevant experimental data at the TeV scale. All Feynman rules of our model, such as vertices, propagators etc., can be computed directly from the effective Lagrangians in the conventional method of perturbative QFT. The aim of the present work is to make a clear and systematic calculation in order to obtain the amplitudes. The analysis is made with the intention of compatibility with other field theoretical models.

The present work is organized as follows, in the Sec. II, we set up our model for pp and $p\bar{p}$ scattering with pomeron spin-2 and odderon spin-3 exchanges. The amplitudes are also computed as well. The observables will be calculated and free parameters of our model will be fitted with the relevant experimental data at the TeV scales in Sec. III. In Sec. IV, we close this work by giving discussions and conclusions.

II. FORMALISMS: MODEL SETUP AND SCATTERING AMPLITUDES

A. Effective Lagrangians of the pp and $p\bar{p}$ scattering in spin-2 pomeron and spin-3 odderon exchange picture

In this section, we will set up the effective Lagrangians of the pp and $p\bar{p}$ scatterings. It is well known that the pomeron exchange plays a major role in elastic proton-proton scattering at high energy but low momentum exchange regimes. For this work, we assume the pomeron as spin-2 tensor particle and the Lagrangian is given by [48,49]

$$\mathcal{L}_{\mathbb{P}} = -ig_{\mathbb{P}}\mathbb{P}^{\mu\nu}\mathcal{G}^{\mu'\nu'}_{\mu\nu}\bar{\psi}\gamma_{\mu'}\overset{\leftrightarrow}{\partial}_{\nu'}\psi, \tag{1}$$

where $\mathbb{P}^{\mu\nu}$ is symmetric spin-2 tensor field, ψ is Dirac proton field, $\bar{\psi}\overset{\leftrightarrow}{\partial}_{\mu}\psi \equiv (\partial_\mu\bar{\psi})\psi - \bar{\psi}\partial_\mu\psi$ and the coupling $g_{\mathbb{P}} = 3 \times 1.87$ GeV^{-1} as used in Ref. [48]. The totally symmetric tensor $\mathcal{G}^{\mu'\nu'}_{\mu\nu}$ is defined by

$$\mathcal{G}^{\mu'\nu'}_{\mu\nu} = \frac{1}{2!}\left(g^{\mu'}_{\mu}g^{\nu'}_{\nu} + g^{\mu'}_{\nu}g^{\nu'}_{\mu}\right). \tag{2}$$

The corresponding vertex function of the pomeron-proton-proton coupling is given by

$$i\Gamma^{\mathbb{P}}_{\mu\nu}(q,q') = -ig_{\mathbb{P}}\mathcal{G}^{\mu'\nu'}_{\mu\nu}\gamma_{\mu'}(q'_{\nu'}+q_{\nu'}), \tag{3}$$

where q and q' are the incoming and outgoing proton/antiproton momenta, respectively.

For the spin-3 odderon exchange interaction, the effective Lagrangian reads

$$\mathcal{L}_{\mathbb{O}} = -\frac{g_{\mathbb{O}}}{\tilde{M}_0}\mathbb{O}^{\mu\nu\rho}\mathcal{G}^{\mu'\nu'\rho'}_{\mu\nu\rho}\bar{\psi}\gamma_{\mu'}\overleftrightarrow{\partial}_{\nu'}\overleftrightarrow{\partial}_{\rho'}\psi, \tag{4}$$

where $\mathbb{O}^{\mu\nu\rho}$ is the spin-3 tensor field that is totally symmetric under the interchanges of the Lorentz indices, i.e., $\mathbb{O}^{\mu\nu\rho} = \mathbb{O}^{\nu\rho\mu} = \mathbb{O}^{\rho\mu\nu} = \mathbb{O}^{\mu\rho\nu} = \mathbb{O}^{\nu\mu\rho} = \mathbb{O}^{\rho\nu\mu}$. In order to obtain the effective Lagrangian in Eq. (4), in addition, we have followed the construction of the higher spin field coupling to the nucleons in Ref. [48] by adding the twist-2 operator as shown in Appendix B of Ref. [48] and all detailed discussions therein. Moreover, the coupling $g_{\mathbb{O}}$ is a free parameter in this work and it carries the same mass dimension as introduced for $g_{\mathbb{P}}$. The $\tilde{M}_0$ is the mass parameter set at $\tilde{M}_0 = 1$ GeV. In the latter, we will see that this parameter is absent in the scattering amplitude and introduced only for proper mass dimension. The totally symmetric tensor $\mathcal{G}^{\mu'\nu'\rho'}_{\mu\nu\rho}$ is used to ensure that the lower indices (μ,ν,ρ) of the vertex functions, $\Gamma^{\mathbb{O}}_{\mu\nu\rho}$ is totally symmetric tensor. It is defined by

$$\mathcal{G}^{\mu'\nu'\rho'}_{\mu\nu\rho} = \frac{1}{3!}\Big(g^{\mu'}_{\mu}g^{\nu'}_{\nu}g^{\rho'}_{\rho} + g^{\mu'}_{\nu}g^{\nu'}_{\rho}g^{\rho'}_{\mu} + g^{\mu'}_{\rho}g^{\nu'}_{\mu}g^{\rho'}_{\nu} + g^{\mu'}_{\nu}g^{\nu'}_{\mu}g^{\rho'}_{\rho} + g^{\mu'}_{\mu}g^{\nu'}_{\rho}g^{\rho'}_{\nu} + g^{\mu'}_{\rho}g^{\nu'}_{\nu}g^{\rho'}_{\mu}\Big). \tag{5}$$

According to the Lagrangian in Eq. (4), we can write the Feynman rules for the vertex function for $\mathcal{L}_{\mathbb{O}}$ as

$$i\Gamma^{\mathbb{O}}_{\mu\nu\rho}(q,q') = -i\frac{g_{\mathbb{O}}}{\tilde{M}_0}\mathcal{G}^{\mu'\nu'\rho'}_{\mu\nu\rho}\gamma_{\mu'}(q'_{\nu'}+q_{\nu'})(q'_{\rho'}+q_{\rho'}), \tag{6}$$

where q and q' represent the incoming and outgoing momenta of the proton/antiproton of the vertex functions.

B. Scattering amplitudes of the pp and $p\bar{p}$ elastic scattering

Next step, we will calculate the amplitudes for the elastic pp and $p\bar{p}$ scattering processes under the external momentum specifications as $p(q_1)p(q_2) \to p(q_3)p(q_4)$ and $\bar{p}(q_1)p(q_2) \to \bar{p}(q_3)p(q_4)$ for pp and $p\bar{p}$ elastic scattering processes, respectively. In addition, we assume that the elastic pp and $p\bar{p}$ scatterings are mainly dominated by the pomeron and odderon exchanges since other mesons and Reggeons exchange contributions are negligibly small in these processes at TeV scale.

By using the standard method in QFT [92], the elastic pp scattering amplitude of the pomeron exchange is given by

$$\begin{aligned} i\mathcal{M}^{pp}_{\mathbb{P}} &= \langle p(q_3)p(q_4)|:\mathcal{T}\exp\left(i\int\mathcal{L}_{\mathbb{P}}(x)d^4x\right):|p(q_1)p(q_2)\rangle, \\ &= -ig^2_{\mathbb{P}}\mathcal{G}^{\mu'_1\nu'_1}_{\mu_1\nu_1}\bar{u}(q_3)\gamma_{\mu'_1}(q_{3,\nu'_1}+q_{1,\nu'_1})u(q_1)i\Delta^{\mu_1\nu_1;\mu_2\nu_2}_{\mathbb{P}}(s,t) \\ &\quad\times\mathcal{G}^{\mu'_2\nu'_2}_{\mu_2\nu_2}\bar{u}(q_4)\gamma_{\mu'_2}(q_{4,\nu'_2}+q_{2,\nu'_2})u(q_2)\mathcal{F}_{\mathbb{P}}(t)^2, \end{aligned} \tag{7}$$

and the elastic $p\bar{p}$ scattering amplitude of the pomeron exchange is given by

$$\begin{aligned} i\mathcal{M}^{p\bar{p}}_{\mathbb{P}} &= \langle \bar{p}(q_3)p(q_4)|:\mathcal{T}\exp\left(i\int\mathcal{L}_{\mathbb{P}}(x)d^4x\right):|\bar{p}(q_1)p(q_2)\rangle, \\ &= -ig^2_{\mathbb{P}}\mathcal{G}^{\mu'_1\nu'_1}_{\mu_1\nu_1}\bar{v}(q_1)\gamma_{\mu'_1}(q_{1,\nu'_1}+q_{3,\nu'_1})v(q_3)i\Delta^{\mu_1\nu_1;\mu_2\nu_2}_{\mathbb{P}}(s,t) \\ &\quad\times\mathcal{G}^{\mu'_2\nu'_2}_{\mu_2\nu_2}\bar{u}(q_4)\gamma_{\mu'_2}(q_{4,\nu'_2}+q_{2,\nu'_2})u(q_2)\mathcal{F}_{\mathbb{P}}(t)^2. \end{aligned} \tag{8}$$

For the propagator of the spin-2 pomeron $\Delta^{\mu\nu;\mu'\nu'}_{\mathbb{P}}$, we employ from Ref. [48] and it takes the following form:

$$i\Delta^{\mu\nu,\rho\sigma}_{\mathbb{P}}(s,t) = \frac{1}{4s}\left[g^{\mu\rho}g^{\nu\sigma}+g^{\mu\sigma}g^{\nu\rho}-\frac{1}{2}g^{\mu\nu}g^{\rho\sigma}\right](-i\alpha'_{\mathbb{P}}s)^{\alpha_{\mathbb{P}}(t)-1}, \tag{9}$$

with the conventional linear pomeron trajectory [48,49]

$$\alpha_{\mathbb{P}}(t) = 1+\epsilon_{\mathbb{P}}+\alpha'_{\mathbb{P}}t, \tag{10}$$

$$\epsilon_{\mathbb{P}} = 0.0808, \quad \text{and} \quad \alpha'_{\mathbb{P}} = 0.25\ \text{GeV}^{-2}, \tag{11}$$

where the terms, $1+\epsilon_{\mathbb{P}}$ and $\alpha'_{\mathbb{P}}$ represent the vertical interception and slope of the pomeron trajectory, respectively. This formulation of the spin-2 pomeron propagator is an alternative approach to studying soft high energy hadronic collisions. This formalism can be reproduced in

several experimental data. In addition, the pomeron propagator with the Donnachie-Landschoff ansatz in Eq. (9) is proposed by Heidelberg group [48]. Finally, the pomeron-$pp/p\bar{p}$ coupling form factor reads

$$\mathcal{F}_{\mathbb{P}}(t)=\left(1-\frac{t}{4m_p^2}\frac{\mu_p}{\mu_N}\right)\left(1-\frac{t}{4m_p^2}\right)^{-1}\left(1-\frac{t}{m_D^2}\right)^{-2},$$
$$\mu_N=\frac{e}{2m_p},\quad \frac{\mu_p}{\mu_N}=2.7928,\quad m_D^2=0.71\ \mathrm{GeV}^2. \tag{12}$$

This form factor is the standard Dirac form factor of proton and it is widely used to study the pp and $p\bar{p}$ scattering. See more details discussions and its consequences of the form factor in Eq. (12) in chapter two of Ref. [93].

We turn to consider the elastic pp and $p\bar{p}$ scattering amplitudes for the spin-3 odderon exchange contribution. Having used the same manner, the pp scattering amplitude is calculated and one finds

$$\begin{aligned}i\mathcal{M}_{\mathbb{O}}^{pp}&=\langle p(q_3)p(q_4)|:\mathcal{T}\exp\left(i\int\mathcal{L}_{\mathbb{O}}(x)d^4x\right):|p(q_1)p(q_2)\rangle,\\&=-\frac{g_{\mathbb{O}}^2}{\tilde{M}_0^2}\mathcal{G}^{\mu_1\nu_1\rho_1}_{\mu\nu\rho}\bar{u}(q_3)\gamma_{\mu_1}(q_{3,\nu_1}+q_{1,\nu_1})(q_{3,\rho_1}+q_{1,\rho_1})\,u(q_1)i\Delta_{\mathbb{O}}^{\mu\nu\rho;\mu'\nu'\rho'}(s,t)\\&\quad\times\mathcal{G}^{\mu_2\nu_2\rho_2}_{\mu'\nu'\rho'}\bar{u}(q_4)\gamma_{\mu_2}(q_{4,\nu_2}+q_{2,\nu_2})(q_{4,\rho_2}+q_{2,\rho_2})\,u(q_2)\mathcal{F}_{\mathbb{O}}(t)^2,\end{aligned} \tag{13}$$

while the amplitude of the $p\bar{p}$ scattering with the odderon exchange reads

$$\begin{aligned}i\mathcal{M}_{\mathbb{O}}^{p\bar{p}}&=\langle\bar{p}(q_3)p(q_4)|:\mathcal{T}\exp\left(i\int\mathcal{L}_{\mathbb{O}}(x)d^4x\right):|\bar{p}(q_1)p(q_2)\rangle,\\&=-\frac{g_{\mathbb{O}}^2}{\tilde{M}_0^2}\mathcal{G}^{\mu_1\nu_1\rho_1}_{\mu\nu\rho}\bar{v}(q_1)\gamma_{\mu_1}(q_{1,\nu_1}+q_{3,\nu_1})(q_{1,\rho_1}+q_{3,\rho_1})\,v(q_3)i\Delta_{\mathbb{O}}^{\mu\nu\rho;\mu'\nu'\rho'}(s,t)\\&\quad\times\mathcal{G}^{\mu_2\nu_2\rho_2}_{\mu'\nu'\rho'}\bar{u}(q_4)\gamma_{\mu_2}(q_{4,\nu_2}+q_{2,\nu_2})(q_{4,\rho_2}+q_{2,\rho_2})\,u(q_2)\mathcal{F}_{\mathbb{O}}(t)^2.\end{aligned} \tag{14}$$

In addition, we have modified the proton form factor in Eq. (12) for the odderon coupling to pp by adding new three free parameters, A, B, and C as

$$\mathcal{F}_{\mathbb{O}}(t)=\left(1-\frac{At}{4m_p^2}\frac{\mu_p}{\mu_N}\right)\left(1-\frac{Bt}{4m_p^2}\right)^{-1}\left(1-\frac{Ct}{m_D^2}\right)^{-2}. \tag{15}$$

The $\Delta_{\mathbb{O}}^{\mu_1\nu_1\rho_1;\mu_2\nu_2\rho_2}(s,t)$ term is the propagator of the spin-3 particle in momentum space. By analogy to the spin-2 tensor pomeron proposed by [48], we introduce the spin-3 tensor odderon propagator with the Donnachie-Lanschoff parametrization and it reads

$$\begin{aligned}i\Delta_{\mathbb{O}}^{\mu\nu\lambda,\rho\sigma\tau}(s,t)=-i\frac{\tilde{M}_0^2}{6s^2}&\left[\sum_C g^{\mu\rho}(g^{\nu\sigma}g^{\lambda\tau}+g^{\nu\tau}g^{\lambda\sigma})\right.\\&\left.-\frac{1}{2}\sum_C g^{\mu\nu}g^{\lambda\rho}g^{\sigma\tau}\right](-i\alpha'_{\mathbb{O}}s)^{\alpha_{\mathbb{O}}(t)-1},\end{aligned} \tag{16}$$

$$\alpha_{\mathbb{O}}(t)=1+\epsilon_{\mathbb{O}}+\alpha'_{\mathbb{O}}t, \tag{17}$$

where $\sum_C$ stands for the sum over all distinct combinations of the Lorentz indices $(\mu\nu\lambda)$ and $(\rho\sigma\tau)$, for instance,

$$\begin{aligned}\sum_C g_{\mu\nu}g_{\lambda\rho}g_{\sigma\tau}&=g_{\mu\nu}g_{\lambda\rho}g_{\sigma\tau}+g_{\mu\nu}g_{\lambda\sigma}g_{\rho\tau}+g_{\mu\nu}g_{\lambda\tau}g_{\rho\sigma}\\&\quad+g_{\mu\lambda}g_{\nu\rho}g_{\sigma\tau}+g_{\mu\lambda}g_{\nu\sigma}g_{\rho\tau}+g_{\mu\lambda}g_{\nu\tau}g_{\rho\sigma}\\&\quad+g_{\nu\lambda}g_{\mu\rho}g_{\sigma\tau}+g_{\nu\lambda}g_{\mu\sigma}g_{\rho\tau}+g_{\nu\lambda}g_{\mu\tau}g_{\rho\sigma}.\end{aligned} \tag{18}$$

The mass parameter $\tilde{M}_0$ is a free parameter in this work and it is introduced in order to correct the mass dimension of the odderon propagator. In addition, we consider the parameters $\epsilon_{\mathbb{O}}$ and $\alpha'_{\mathbb{O}}$ as free parameters. However, the condition $\epsilon_{\mathbb{O}}<\epsilon_{\mathbb{P}}$ is imposed due to the fact from the experimental data that the total cross sections of both pp and $p\bar{p}$ are identical at very high energies. In the other words, the pomeron exchange contributions for elastic pp and $p\bar{p}$ scattering at the Regge limit always dominate over odderon. Moreover, the tensor structure of the spin-3 odderon propagator has been constructed in Ref. [94]. We close this section by giving the definitions of the four-momentum conservation, the on-shell mass of the particles, and the Mandelstam variables as

$$q_1+q_2=q_3+q_4,\qquad q_1^2=q_2^2=q_3^2=q_4^2=m_p^2,\qquad s+t+u=4m_p^2,$$
$$s=(q_1+q_2)^2=(q_3+q_4)^2,\qquad t=(q_3-q_1)^2=(q_4-q_2)^2,\qquad u=(q_4-q_1)^2=(q_3-q_2)^2. \tag{19}$$

In the next section, we will provide the analytical expressions of the differential cross section for the pp and $p\bar{p}$ elastic scattering with pomeron and odderon exchanges and fit the model parameters with the experimental data of the pp and $p\bar{p}$ elastic scatterings at TeV scale.

III. RESULTS AND DISCUSSIONS

A. Differential cross section formulas

In this subsection, we will provide the analytical formulae of the differential cross section with respect to the t variable and then the model parameters in the present work will be determined by fitting with all available experimental data of the pp and $p\bar{p}$ elastic scatterings at TeV level. The differential cross section of the pp and $p\bar{p}$ scattering is given by [49],

$$\frac{d\sigma^{pp/p\bar{p}}}{dt}=\frac{1}{16\pi s(s-m_p^2)}\frac{1}{4}\sum_{\text{spin}}|\mathcal{M}^{pp/p\bar{p}}|^2. \tag{20}$$

First of all, let us briefly discuss the definitions of the scattering amplitudes of pp and $p\bar{p}$ in the pomeron and odderon exchange picture. Considering the amplitude $\mathcal{M}^{ab}(s,t)$ of an elastic scattering for the $a+b\to a+b$ process in s channel. While the corresponding elastic scattering by crossing to the u channel as $a+\bar{b}\to a+\bar{b}$ with the amplitude $\mathcal{M}^{a\bar{b}}(u,t)$. According to the crossing symmetry of the scattering amplitudes, they are symmetric under interchange between the Mandelstam variables, s and u, as

$$\mathcal{M}^{a\bar{b}}(s,t,u)=\mathcal{M}^{ab}(u,t,s). \tag{21}$$

Moreover, the amplitude $\mathcal{M}_\pm$ is defined from $\mathcal{M}^{ab/a\bar{b}}$ as

$$\mathcal{M}_\pm(s,t)=\frac{1}{2}(\mathcal{M}^{ab}(s,t)\pm\mathcal{M}^{a\bar{b}}(s,t)). \tag{22}$$

Interchange $s\to u$, one finds that the amplitude $\mathcal{M}_+$ is invariant under the crossing symmetry whereas the amplitude $\mathcal{M}_-$ changes the relative sign. We therefore call $\mathcal{M}_+$ and $\mathcal{M}_-$ as even and odd under the crossing symmetry. As a result, one observes that the $\mathcal{M}_+$ and $\mathcal{M}_-$ correspond to the even and odd under charge conjugation, respectively. Since the interchange $s\to u$ is equivalent to charge conjugation transformation ($\mathcal{C}$), i.e., changing particle-particle scattering to particle-antiparticle scattering. We therefore identify $\mathcal{M}_+$ and $\mathcal{M}_-$ as pomeron ($\mathcal{M}_{\mathbb{P}}$ with $\mathcal{C}=+1$) and odderon ($\mathcal{M}_{\mathbb{O}}$ with $\mathcal{C}=-1$) exchange amplitudes, respectively.

As discussed above, we can define the total amplitude of the elastic pp and $p\bar{p}$ processes with pomeron and odderon exchange diagrams at the tree level as follow

$$\mathcal{M}^{pp}=\mathcal{M}_{\mathbb{P}}^{pp}-\mathcal{M}_{\mathbb{O}}^{pp}, \tag{23}$$

$$\mathcal{M}^{p\bar{p}}=\mathcal{M}_{\mathbb{P}}^{p\bar{p}}+\mathcal{M}_{\mathbb{O}}^{p\bar{p}}. \tag{24}$$

The absolute square amplitudes of $\mathcal{M}^{pp}$ and $\mathcal{M}^{p\bar{p}}$, averaged over unpolarized initial spin states of incoming particles, are given by

$$\sum_{\text{spin}}|\mathcal{M}^{pp}|^2=\sum_{\text{spin}}(|\mathcal{M}_{\mathbb{P}}^{pp}|^2-|\mathcal{M}_{\mathbb{P}}^{pp}\mathcal{M}_{\mathbb{O}}^{pp*}|-|\mathcal{M}_{\mathbb{P}}^{pp*}\mathcal{M}_{\mathbb{O}}^{pp}|+|\mathcal{M}_{\mathbb{O}}^{pp}|^2), \tag{25}$$

$$\text{and}\quad \sum_{\text{spin}}|\mathcal{M}^{p\bar{p}}|^2=\sum_{\text{spin}}(|\mathcal{M}_{\mathbb{P}}^{p\bar{p}}|^2+|\mathcal{M}_{\mathbb{P}}^{p\bar{p}*}\mathcal{M}_{\mathbb{O}}^{p\bar{p}}|+|\mathcal{M}_{\mathbb{P}}^{p\bar{p}}\mathcal{M}_{\mathbb{O}}^{p\bar{p}*}|+|\mathcal{M}_{\mathbb{O}}^{p\bar{p}}|^2). \tag{26}$$

The explicit forms of the absolute square amplitudes with an average sum over initial states can be calculated in the following forms:

$$\begin{aligned}\sum_{\text{spin}}|\mathcal{M}_{\mathbb{P}}^{pp}|^2=&\,\text{Tr}\Big[(\not{q}_3+m_p)\gamma_{\mu_1'}(q_{3,\nu_1'}+q_{1,\nu_1'})(\not{q}_1+m_p)\gamma_{\mu_3'}(q_{3,\nu_3'}+q_{1,\nu_3'})\\&\times(\not{q}_4+m_p)\gamma_{\mu_2'}(q_{4,\nu_2'}+q_{2,\nu_2'})(\not{q}_2+m_p)\gamma_{\mu_4'}(q_{4,\nu_4'}+q_{2,\nu_4'})\Big]\\&\times g_{\mathbb{P}}^4\mathcal{G}_{\mu_1\nu_1}^{\mu_1'\nu_1'}\mathcal{G}_{\mu_3\nu_3}^{\mu_3'\nu_3'}\mathcal{G}_{\mu_2\nu_2}^{\mu_2'\nu_2'}\mathcal{G}_{\mu_4\nu_4}^{\mu_4'\nu_4'}\Delta_{\mathbb{P}}^{\mu_1\nu_1;\mu_2\nu_2}(s,t)\Delta_{\mathbb{P}}^{\mu_3\nu_3;\mu_4\nu_4}(s,t)\,\mathcal{F}_{\mathbb{P}}(t)^4\\\approx&\,\frac{16g_{\mathbb{P}}^4\left[1-\frac{t}{4m_p^2}\frac{\mu_p}{\mu_N}\right]^4}{\left[1-\frac{t}{m_p^2}\right]^4\left[1-\frac{t}{m_D^2}\right]^8}s^2(\alpha_{\mathbb{P}}'s)^{2\epsilon_{\mathbb{P}}+2\alpha_{\mathbb{P}}'t},\end{aligned} \tag{27}$$

$$\sum_{\text{spin}}|\mathcal{M}_{\mathbb{O}}^{pp}|^2 = \text{Tr}\Big[(\not{q}_3+m_p)\gamma_{\mu_1}(q_{3,\nu_1}+q_{1,\nu_1})(q_{3,\rho_1}+q_{1,\rho_1})(\not{q}_1+m_p)\gamma_{\bar{\mu}_3}(q_{3,\bar{\nu}_3}+q_{1,\bar{\nu}_3})(q_{3,\bar{\rho}_3}+q_{1,\bar{\rho}_3})$$
$$\times(\not{q}_4+m_p)\gamma_{\mu_2}(q_{4,\nu_2}+q_{2,\nu_2})(q_{4,\rho_2}+q_{2,\rho_2})(\not{q}_2+m_p)\gamma_{\bar{\mu}_4}(q_{4,\bar{\nu}_4}+q_{2,\bar{\nu}_4})(q_{4,\bar{\rho}_4}+q_{2,\bar{\rho}_4})\Big]$$
$$\times\frac{g_{\mathbb{O}}^4}{\tilde{M}_0^4}\mathcal{G}_{\mu\nu\rho}^{\mu_1\nu_1\rho_1}\mathcal{G}_{\bar{\mu}\bar{\nu}\bar{\rho}}^{\bar{\mu}_3\bar{\nu}_3\bar{\rho}_3}\mathcal{G}_{\mu'\nu'\rho'}^{\mu_2\nu_2\rho_2}\mathcal{G}_{\bar{\mu}'\bar{\nu}'\bar{\rho}'}^{\bar{\mu}_4\bar{\nu}_4\bar{\rho}_4}\Delta_{\mathbb{O}}^{\mu\nu\rho;\mu'\nu'\rho'}(s,t)\Delta_{\mathbb{O}}^{\bar{\mu}\bar{\nu}\bar{\rho};\bar{\mu}'\bar{\nu}'\bar{\rho}'}(s,t)\mathcal{F}_{\mathbb{O}}(t)^4$$
$$\approx\frac{64g_{\mathbb{O}}^4\left[1-\frac{At}{4m_p^2}\frac{\mu_p}{\mu_N}\right]^4}{9\left[1-\frac{Bt}{m_p^2}\right]^4\left[1-\frac{Ct}{m_D^2}\right]^8}s^2(\alpha'_{\mathbb{O}}s)^{2\epsilon_{\mathbb{O}}+2\alpha'_{\mathbb{O}}t}, \tag{28}$$

$$\sum_{\text{spin}}|\mathcal{M}_{\mathbb{P}}^{pp}\mathcal{M}_{\mathbb{O}}^{pp*}| = \text{Tr}\Big[(\not{q}_3+m_p)\gamma_{\mu'_1}(q_{3,\nu'_1}+q_{1,\nu'_1})(\not{q}_1+m_p)\gamma_{\bar{\mu}_3}(q_{3,\bar{\nu}_3}+q_{1,\bar{\nu}_3})(q_{3,\bar{\rho}_3}+q_{1,\bar{\rho}_3})$$
$$\times(\not{q}_4+m_p)\gamma_{\mu'_2}(q_{4,\nu'_2}+q_{2,\nu'_2})(\not{q}_2+m_p)\gamma_{\bar{\mu}_4}(q_{4,\bar{\nu}_4}+q_{2,\bar{\nu}_4})(q_{4,\bar{\rho}_4}+q_{2,\bar{\rho}_4})\Big]$$
$$\times\frac{g_{\mathbb{P}}^2g_{\mathbb{O}}^2}{\tilde{M}_0^2}\mathcal{G}_{\mu_1\nu_1}^{\mu'_1\nu'_1}\mathcal{G}_{\bar{\mu}\bar{\nu}\bar{\rho}}^{\bar{\mu}_3\bar{\nu}_3\bar{\rho}_3}\mathcal{G}_{\mu_2\nu_2}^{\mu'_2\nu'_2}\mathcal{G}_{\bar{\mu}'\bar{\nu}'\bar{\rho}'}^{\bar{\mu}_4\bar{\nu}_4\bar{\rho}_4}\Delta_{\mathbb{P}}^{\mu_1\nu_1;\mu_2\nu_2}(s,t)\Delta_{\mathbb{O}}^{\bar{\mu}\bar{\nu}\bar{\rho};\bar{\mu}'\bar{\nu}'\bar{\rho}'}(s,t)\mathcal{F}_{\mathbb{P}}(t)^2\mathcal{F}_{\mathbb{O}}(t)^2$$
$$\approx\frac{32g_{\mathbb{P}}^2g_{\mathbb{O}}^2\left[1-\frac{t}{4m_p^2}\frac{\mu_p}{\mu_N}\right]^2\left[1-\frac{At}{4m_p^2}\frac{\mu_p}{\mu_N}\right]^2}{9\left[1-\frac{t}{m_p^2}\right]^2\left[1-\frac{t}{m_D^2}\right]^4\left[1-\frac{Bt}{m_p^2}\right]^2\left[1-\frac{Ct}{m_D^2}\right]^4}s^2(-i\alpha'_{\mathbb{P}}s)^{\epsilon_{\mathbb{P}}+\alpha'_{\mathbb{P}}t}(i\alpha'_{\mathbb{O}}s)^{\epsilon_{\mathbb{O}}+\alpha'_{\mathbb{O}}t}, \tag{29}$$

$$\sum_{\text{spin}}|\mathcal{M}_{\mathbb{P}}^{p\bar{p}}|^2 = \text{Tr}\Big[(\not{q}_1-m_p)\gamma_{\mu'_1}(q_{3,\nu'_1}+q_{1,\nu'_1})(\not{q}_3-m_p)\gamma_{\mu'_3}(q_{3,\nu'_3}+q_{1,\nu'_3})$$
$$\times(\not{q}_4+m_p)\gamma_{\mu'_2}(q_{4,\nu'_2}+q_{2,\nu'_2})(\not{q}_2+m_p)\gamma_{\mu'_4}(q_{4,\nu'_4}+q_{2,\nu'_4})\Big]$$
$$\times g_{\mathbb{P}}^4\mathcal{G}_{\mu_1\nu_1}^{\mu'_1\nu'_1}\mathcal{G}_{\mu_3\nu_3}^{\mu'_3\nu'_3}\mathcal{G}_{\mu_2\nu_2}^{\mu'_2\nu'_2}\mathcal{G}_{\mu_4\nu_4}^{\mu'_4\nu'_4}\Delta_{\mathbb{P}}^{\mu_1\nu_1;\mu_2\nu_2}(s,t)\Delta_{\mathbb{P}}^{\mu_3\nu_3;\mu_4\nu_4}(s,t)\mathcal{F}_{\mathbb{P}}(t)^4$$
$$\approx\frac{16g_{\mathbb{P}}^4\left[1-\frac{t}{4m_p^2}\frac{\mu_p}{\mu_N}\right]^4}{\left[1-\frac{t}{m_p^2}\right]^4\left[1-\frac{t}{m_D^2}\right]^8}s^2(\alpha'_{\mathbb{P}}s)^{2\epsilon_{\mathbb{P}}+2\alpha'_{\mathbb{P}}t}, \tag{30}$$

$$\sum_{\text{spin}}|\mathcal{M}_{\mathbb{O}}^{p\bar{p}}|^2 = \text{Tr}\Big[(\not{q}_1-m_p)\gamma_{\mu_1}(q_{3,\nu_1}+q_{1,\nu_1})(q_{3,\rho_1}+q_{1,\rho_1})(\not{q}_3-m_p)\gamma_{\bar{\mu}_3}(q_{3,\bar{\nu}_3}+q_{1,\bar{\nu}_3})(q_{3,\bar{\rho}_3}+q_{1,\bar{\rho}_3})$$
$$\times(\not{q}_4+m_p)\gamma_{\mu_2}(q_{4,\nu_2}+q_{2,\nu_2})(q_{4,\rho_2}+q_{2,\rho_2})(\not{q}_2+m_p)\gamma_{\bar{\mu}_4}(q_{4,\bar{\nu}_4}+q_{2,\bar{\nu}_4})(q_{4,\bar{\rho}_4}+q_{2,\bar{\rho}_4})\Big]$$
$$\times\frac{g_{\mathbb{O}}^4}{\tilde{M}_0^4}\mathcal{G}_{\mu\nu\rho}^{\mu_1\nu_1\rho_1}\mathcal{G}_{\bar{\mu}\bar{\nu}\bar{\rho}}^{\bar{\mu}_3\bar{\nu}_3\bar{\rho}_3}\mathcal{G}_{\mu'\nu'\rho'}^{\mu_2\nu_2\rho_2}\mathcal{G}_{\bar{\mu}'\bar{\nu}'\bar{\rho}'}^{\bar{\mu}_4\bar{\nu}_4\bar{\rho}_4}\Delta_{\mathbb{O}}^{\mu\nu\rho;\mu'\nu'\rho'}(s,t)\Delta_{\mathbb{O}}^{\bar{\mu}\bar{\nu}\bar{\rho};\bar{\mu}'\bar{\nu}'\bar{\rho}'}(s,t)\mathcal{F}_{\mathbb{O}}(t)^4$$
$$\approx\frac{64g_{\mathbb{O}}^4\left[1-\frac{At}{4m_p^2}\frac{\mu_p}{\mu_N}\right]^4}{9\left[1-\frac{Bt}{m_p^2}\right]^4\left[1-\frac{Ct}{m_D^2}\right]^8}s^2(\alpha'_{\mathbb{O}}s)^{2\epsilon_{\mathbb{O}}+2\alpha'_{\mathbb{O}}t}, \tag{31}$$

$$\begin{aligned}\sum_{\text{spin}}|\mathcal{M}_{\mathbb{P}}^{p\bar{p}}\mathcal{M}_{\mathbb{O}}^{p\bar{p}*}|^2 &= \text{Tr}\Big[(\not{q}_1-m_p)\gamma_{\mu_1'}(q_{3,\nu_1'}+q_{1,\nu_1'})(\not{q}_3-m_p)\gamma_{\bar{\mu}_3}(q_{3,\bar{\nu}_3}+q_{1,\bar{\nu}_3})(q_{3,\bar{\rho}_3}+q_{1,\bar{\rho}_3})\\ &\times(\not{q}_4+m_p)\gamma_{\mu_2'}(q_{4,\nu_2'}+q_{2,\nu_2'})(\not{q}_2+m_p)\gamma_{\bar{\mu}_4}(q_{4,\bar{\nu}_4}+q_{2,\bar{\nu}_4})(q_{4,\bar{\rho}_4}+q_{2,\bar{\rho}_4})\Big]\\ &\times\frac{g_{\mathbb{P}}^2g_{\mathbb{O}}^2}{\tilde{M}_0^2}\mathcal{G}_{\mu_1\nu_1}^{\mu_1'\nu_1'}\mathcal{G}_{\bar{\mu}\bar{\nu}\bar{\rho}}^{\bar{\mu}_3\bar{\nu}_3\bar{\rho}_3}\mathcal{G}_{\mu_2\nu_2}^{\mu_2'\nu_2'}\mathcal{G}_{\bar{\mu}'\bar{\nu}'\bar{\rho}'}^{\bar{\mu}_4\bar{\nu}_4\bar{\rho}_4}\Delta_{\mathbb{P}}^{\mu_1\nu_1;\mu_2\nu_2}(s,t)\Delta_{\mathbb{O}}^{\bar{\mu}\bar{\nu}\bar{\rho};\bar{\mu}'\bar{\nu}'\bar{\rho}'}(s,t)\mathcal{F}_{\mathbb{P}}(t)^2\mathcal{F}_{\mathbb{O}}(t)^2\\ &\approx\frac{32g_{\mathbb{P}}^2g_{\mathbb{O}}^2\left[1-\frac{t}{4m_p^2}\frac{\mu_p}{\mu_N}\right]^2\left[1-\frac{At}{4m_p^2}\frac{\mu_p}{\mu_N}\right]^2}{9\left[1-\frac{t}{m_p^2}\right]^2\left[1-\frac{t}{m_D^2}\right]^4\left[1-\frac{Bt}{m_p^2}\right]^2\left[1-\frac{Ct}{m_D^2}\right]^4}s^2(-i\alpha_{\mathbb{P}}'s)^{\epsilon_{\mathbb{P}}+\alpha_{\mathbb{P}}'t}(i\alpha_{\mathbb{O}}'s)^{\epsilon_{\mathbb{O}}+\alpha_{\mathbb{O}}'t},\end{aligned}\tag{32}$$

where the Regge limit, $s\gg t,m_p^2$ has been applied for the approximations to obtain the final results. Here we have used the following normalizations and sum over spin of the spinors as

$$\begin{aligned}\bar{u}_r(p,m_p)u_s(p,m_p)&=2m_p\delta_{rs}, &\sum_r u_r(p,m_p)\bar{u}_r(p,m_p)&=\not{p}+m_p,\\ \bar{v}_r(p,m_p)v_s(p,m_p)&=-2m_p\delta_{rs}, &\sum_r v_r(p,m_p)\bar{v}_r(p,m_p)&=\not{p}-m_p,\end{aligned}\tag{33}$$

where r and s are spin indices of the spinors. As results, we note that $\sum_{\text{spin}}|\mathcal{M}_X^{pp}|^2=\sum_{\text{spin}}|\mathcal{M}_X^{p\bar{p}}|^2$ with $X=\mathbb{P},\mathbb{O}$.

Next, we will present the scalar amplitudes of the pomeron and odderon exchanges as $\mathcal{A}_{\mathbb{P}}$ and $\mathcal{A}_{\mathbb{O}}$, respectively. Having used the results in Eqs. (27) and (28), they are written as

$$\mathcal{A}_{\mathbb{P}}(s,t)=4g_{\mathbb{P}}^2\mathcal{F}_{\mathbb{P}}^2(s,t)(-is\alpha_{\mathbb{P}}')^{\alpha_{\mathbb{P}}'t+\epsilon_{\mathbb{P}}}s,\tag{34}$$

$$\mathcal{A}_{\mathbb{O}}(s,t)=\frac{8}{3}g_{\mathbb{O}}^2\mathcal{F}_{\mathbb{O}}^2(s,t)(-is\alpha_{\mathbb{O}}')^{\alpha_{\mathbb{O}}'t+\epsilon_{\mathbb{O}}}s,\tag{35}$$

where $\mathcal{F}_{\mathbb{O}}^2(s,t)$ and $\mathcal{F}_{\mathbb{O}}^2(s,t)$ are defined by Eqs. (12) and (15), respectively. Here the amplitude of the pp scattering is given by

$$\mathcal{A}^{pp}(s,t)=\mathcal{A}_{\mathbb{P}}(s,t)-\mathcal{A}_{\mathbb{O}}(s,t).\tag{36}$$

According to the optical theorem, one can write the total cross section formula as

$$\begin{aligned}\sigma_{\text{tot}}^{pp}&=\frac{1}{s}\text{Im}\mathcal{A}^{pp}(s,0)=\frac{1}{s}\text{Im}[\mathcal{A}_{\mathbb{P}}(s,0)-\mathcal{A}_{\mathbb{O}}(s,0)]\\ &=\text{Im}\left[4g_{\mathbb{P}}^2(-i\alpha_{\mathbb{P}}'s)^{\epsilon_{\mathbb{P}}}-\frac{8}{3}g_{\mathbb{O}}^2(-i\alpha_{\mathbb{O}}'s)^{\epsilon_{\mathbb{O}}}\right].\end{aligned}\tag{37}$$

In the following subsection, we will use the total cross section in Eq. (37) to compare with the data from the TOTEM collaboration at the TeV scale after the model parameters are chosen.

B. Parameters fitting and discussion

In this section, we perform curve fitting of the model parameters with experimental data. As mentioned in Sec. II, we have six free parameters, i.e., the odderon-pp coupling constant $g_{\mathbb{O}}$, $\epsilon_{\mathbb{O}}$, $\alpha_{\mathbb{O}}'$ and the modified odderon-pp form-factor parameters A, B, and C. The observed value for differential cross sections of pp and $p\bar{p}$ scattering, $d\sigma^{\text{obs}}/dt$, come from various experiments with the center of mass energy ranging from 1.8 TeV [95] for $p\bar{p}$, 1.96 TeV [81] for pp and [80] for $p\bar{p}$, 2.76 TeV [96] with 13σ and 4.3σ, and 7 TeV [97] and 13 TeV [98] for pp scattering. Since we are interested in the small $-t$ limit, we only use the observed data with the linear relation between the differential cross section and the momentum exchange because the effect of the pomeron and odderon is highly manifested in the linear regime of the differential cross section. We define χ^2 function as

$$\chi^2(\alpha_i)=\sum_{j=1}^{N}\left(\frac{\frac{d\sigma}{dt}(\alpha_i)_j^{\text{model}}-\frac{d\sigma^{\text{obs}}}{dt\,j}}{\frac{d\sigma^{\text{obs}}}{dt\,j}}\right)^2,\tag{38}$$

where α_i are six parameters $(g_{\mathbb{O}},\epsilon_{\mathbb{O}},\alpha_{\mathbb{O}}',A,B,C)$ and $j=1,\ldots,N$ is the index of the data points associated with the momentum exchange, $-t$. In order to obtain the best fit parameters, we minimize χ^2 functions using IMINUIT [99,100]. The results are shown in the Table I. Note that the errors are calculated using the Hessian matrix where more details will be provided in the Appendix.

The central values of $g_{\mathbb{O}}$, $\alpha_{\mathbb{O}}'$, $\epsilon_{\mathbb{O}}$, A, B, and C are consistent among various datasets. The odderon mass can

TABLE I. Summary of best fit parameters for each dataset.

Description	χ^2	d.o.f	$g_{\mathbb{O}}$	$\alpha'_{\mathbb{O}}$	$\epsilon_{\mathbb{O}}$
1.80 TeV $p\bar{p}$ [95]	0.076	49	9.346($\pm$0.563)	0.188($\pm$0.040)	0.055($\pm$0.009)
1.96 TeV $p\bar{p}$ [80], pp [81]	0.516	17	14.927($\pm$1.754)	0.158($\pm$0.036)	0.064($\pm$0.018)
2.76 TeV pp [96] (13σ)	0.036	12	25.114($\pm$3.574)	0.199($\pm$0.042)	0.070($\pm$0.020)
7.00 TeV pp [97]	0.048	83	9.888($\pm$0.468)	0.200($\pm$0.047)	0.060($\pm$0.006)
13.0 TeV pp [98]	0.009	150	9.725($\pm$0.346)	0.200($\pm$0.024)	0.063($\pm$0.004)
Averages			13.800($\pm$1.112)	0.189($\pm$0.038)	0.062($\pm$0.011)
Description	A		B	C	$m_{\mathbb{O}}$
1.80 TeV $p\bar{p}$ [95]	$-1.340(\pm0.193)$		0.242($\pm$0.262)	0.436($\pm$0.117)	3.213($\pm$0.611)
1.96 TeV $p\bar{p}$ [80], pp [81]	$-0.855(\pm0.195)$		1.448($\pm$0.394)	1.044($\pm$0.151)	3.497($\pm$0.884)
2.76 TeV pp [96] (13σ)	$-1.430(\pm0.167)$		7.730($\pm$1.374)	0.064($\pm$0.113)	3.112($\pm$0.773)
7.00 TeV pp [97]	$-2.388(\pm0.265)$		$-0.060(\pm0.312)$	0.469($\pm$0.144)	3.116($\pm$0.519)
13.0 TeV pp [98]	$-2.342(\pm0.145)$		$-0.087(\pm0.175)$	0.455($\pm$0.082)	3.113($\pm$0.291)
Averages	$-1.671(\pm0.221)$		1.855(±-2.121)	0.493($\pm$0.264)	3.201($\pm$0.609)

be calculated from its Regge trajectory at the pole, $t = m_{\mathbb{O}}^2$ with $\alpha_{\mathbb{O}}(m_{\mathbb{O}}^2) = J = 3$ as

$$m_{\mathbb{O}}(J=3) = \sqrt{\frac{J-1-\epsilon_{\mathbb{O}}}{\alpha'_{\mathbb{O}}}}\Bigg|_{J=3}, \tag{39}$$

which is consistent due to its dependency on $\epsilon_{\mathbb{O}}$ and $\alpha'_{\mathbb{O}}$.

The quality of parameter fitting can be determined using the minimized χ^2 per degree of freedom. Among the available datasets, the best parameters with sufficient statistics come from the pp-TOTEM 13 TeV data. However, using this particular data alone leads to an overfitting problem; i.e., these parameters lead to unsatisfying fits with $p\bar{p}$ datasets. We, therefore, take a more global analysis using the combined χ^2 function of all available datasets. We then use the parameter fitting from the combined dataset as the representation of our model. The model differential cross sections comparing with experimental data are shown in Fig. 1. We have provided the statistical error analysis in detail in the Appendix.

By using the Eq. (39) with the best-fit parameters, $\epsilon_{\mathbb{O}}$ and $\alpha'_{\mathbb{O}}$ from the combined dataset, one can determine the masses of the odderons with $J = 3, 5, 7$ as shown below,

$$\begin{aligned} m_{\mathbb{O}}(J^{PC} = 3^{--}) &= 3.201 \pm 0.609 \text{ GeV}, \\ m_{\mathbb{O}}(J^{PC} = 5^{--}) &= 4.563 \pm 0.868 \text{ GeV}, \\ m_{\mathbb{O}}(J^{PC} = 7^{--}) &= 5.603 \pm 1.066 \text{ GeV}. \end{aligned} \tag{40}$$

We note that the lowest mass (pole position) of the tensor odderon with spin-3 is around 3 GeV. In addition, the Chew-Frautschi plot of the odderon Regge trajectory is depicted in Fig. 2. The odderon mass results in the present work are consistent with Ref. [52]. In that work, the authors considered the odderons as the oddballs in the double pole Regge model with spin-3, -5, and -7. Then, the masses of the odderon are extracted from the experimental data. According to the literature review, we found that the theoretical estimation such as SU(3) lattice QCD for isotropic and anisotropic cases [24,25,45], Wilson loop approach [30], vacuum correlation method in QCD [28,29], QCD sum rules [21,82,83], relativistic many body framework [46] give the ranges of odderon masses as 3.5–4.5 GeV for spin-3, 5.0–5.5 GeV for spin-5, and 6.0–6.5 GeV for spin-7. We note that the theoretical model estimations in the literature of the odderon masses are a bit heavier than the mass estimations from the data in this work by about 0.3 GeV. However, the spin-3 odderon mass from the double pole Regge model gives $m_{\mathbb{O}}^{DP} = 3.001$ GeV [52] which is lighter than our work. From the results in Table I, the odderon trajectory slope, $\alpha'_{\mathbb{O}} = 0.189$ GeV^{-2}, and the pomeron slope, $\alpha'_{\mathbb{P}} = 0.25$ GeV^{-2}, coming from Donnachie-Landshoff fit [13,14] are compatible with approximation $\alpha'_{\mathbb{O}} \approx \alpha'_{\mathbb{P}}$.

On the other hand, we obtain $\epsilon_{\mathbb{O}} = 0.0620 \ll 1$. As a result, the best-fit value of $\alpha'_{\mathbb{O}}$ and $\epsilon_{\mathbb{O}}$ in this work correspond to the assumptions in Ref. [48] that $\alpha'_{\mathbb{O}} \approx \alpha'_{\mathbb{P}}$ and $\epsilon_{\mathbb{O}} \leq \epsilon_{\mathbb{P}} (= 0.0808)$, which we use for fixing the parameters $\alpha'_{\mathbb{O}}$ and $\epsilon_{\mathbb{O}}$ due to the lack of data used to constrain at that moment.

It is important to discuss the ability of our spin-3 odderon model to explain the measured small value of the ρ parameter [101], by considering the interference of the real part with the Coulomb interaction at very small t. The ρ parameter is defined by

$$\rho(s,t) = \frac{\text{Re}[\mathcal{A}^{pp}(s,t)]}{\text{Im}[\mathcal{A}^{pp}(s,t)]}, \tag{41}$$

where the $\mathcal{A}^{pp}(s,t)$ is given by Eq. (36). In order to explain the amplitudes of our model in the near-forward angle

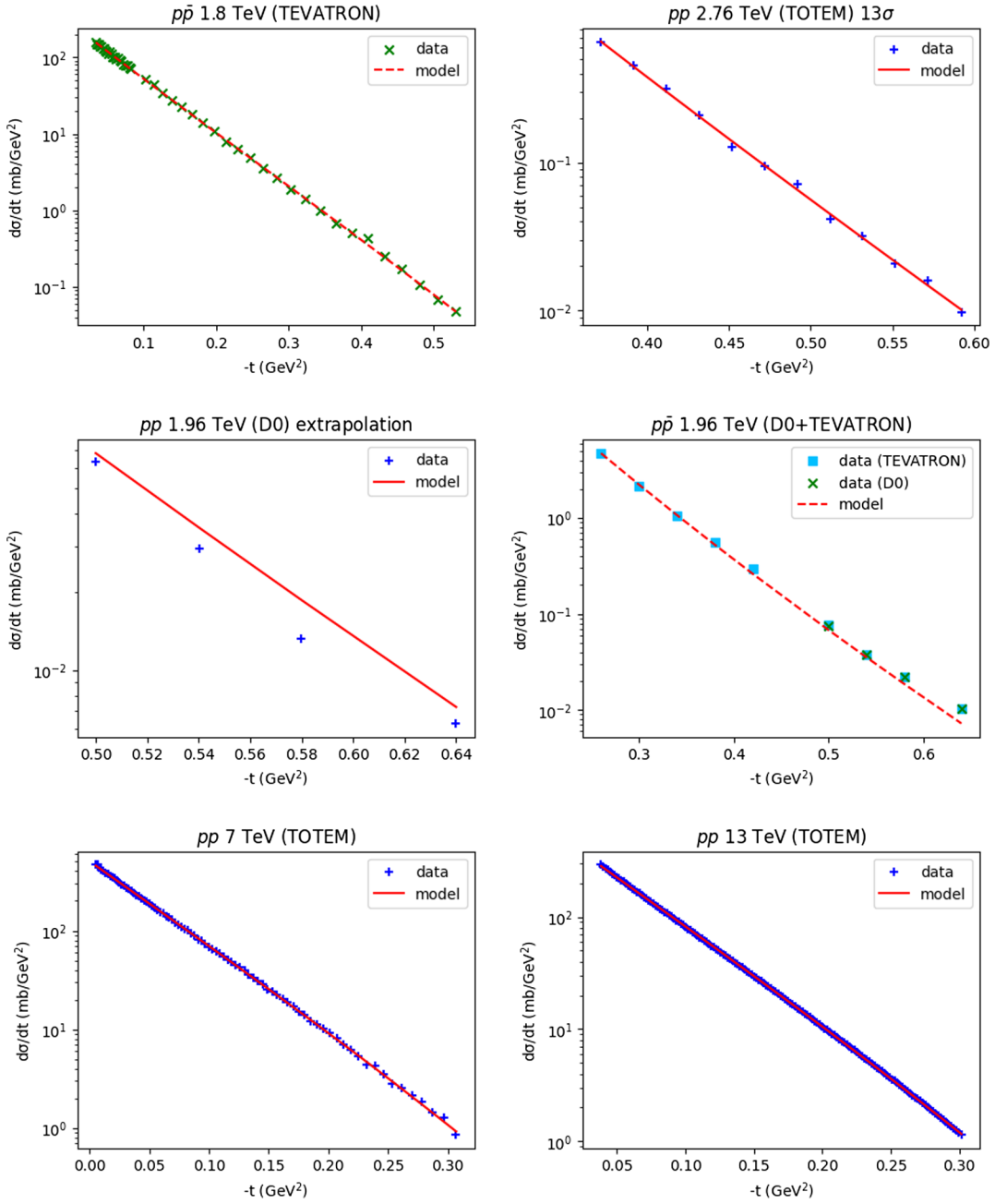

FIG. 1. The best fit plots of the differential cross section of the pp (blue plots) and $p\bar{p}$ (green plots) vs the model results with the parameters from the combined dataset fit.

region of $\mathrm{Re}[\mathcal{A}^{pp}(s,t)]$, we follow the argument presented in Ref. [102]. We first discuss Martin's assumption [103,104] that is used to explain the so-called geometric scaling of the real part of the nuclear amplitude, $\mathcal{A}(s,t)$, in the near-forward direction of pp elastic scattering. It has been shown in Refs. [102,103] that

$$\mathrm{Re}[\mathcal{A}(s,T)] = \rho(s,T)\mathrm{Im}[\mathcal{A}(s,T)] + T\frac{d}{dT}\mathrm{Im}[\mathcal{A}(s,T)], \quad (42)$$

where we defined $T \equiv -t$. We note that the imaginary part of the nuclear amplitude, is zero at $T = T_I$, i.e., $\mathrm{Im}[\mathcal{A}(s,T_I)] = 0$. Integrating Eq. (42), one finds

$$\int_0^{T_I} \mathrm{Re}[\mathcal{A}(s,T)]dT = \rho(s,T)T\,\mathrm{Im}[\mathcal{A}(s,T)]|_{T=0}^{T=T_I} = 0. \quad (43)$$

The expression above implies that the imaginary part of $\mathrm{Im}[\mathcal{A}(s,0)] > 0$, which means that the real part of the nuclear amplitude must change sign between $T = 0$ and $T = T_I$. This leads to

$$\mathrm{Re}[\mathcal{A}(s,T_R)] = 0, \quad \text{where } 0 < T_R < T_I. \quad (44)$$

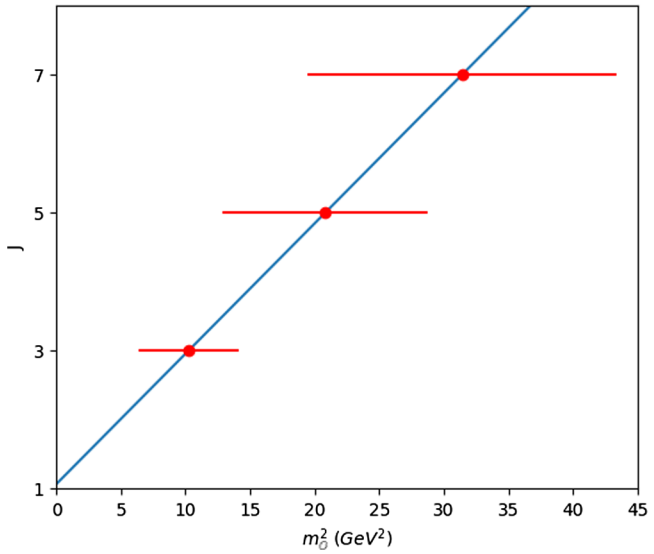

FIG. 2. The Chew-Frautschi plot of the odderon Regge trajectory is depicted by using the $\alpha'_{\mathbb{O}} = 0.189$ GeV^{-2} and $\epsilon_{\mathbb{O}} = 0.062$ from combined data set fitting in Table I. The masses of the odderon with spin-3, -5, and -7 including the error of the fitting parameter estimations with red dots are given by Eq. (40).

In order to obtain a nuclear amplitude that is compatible with experimental data for Coulomb-nuclear interference region, the nuclear amplitude should demonstrate geometric scaling. When we apply the amplitude provided by our model in Eq. (36) in combination with the fitted parameters shown in Table I, we notice that the numerical outcomes of the real and imaginary parts of Eq. (36) do not satisfy the geometric scaling condition. According to this condition, both real and imaginary parts should be positive at small T. Specifically in our model, the imaginary part begins from a positive value at $t = 0$, whereas the real part starts from a negative value. Therefore, to satisfy the geometric scaling, the amplitude in Eq. (36) requires a phase rotation (for example, the Berger-Phillips model was modified in Ref. [102]). To obtain the correct geometric scaling of our nuclear amplitude based on Martin's assumption, we apply the phase factor to the original amplitude in Eq. (36). The resulting amplitude is denoted by $\tilde{\mathcal{A}}^{pp}(s,t)$ and it reads

$$\begin{aligned}\tilde{\mathcal{A}}^{pp}(s,t) &= e^{i\Phi(s,t)}\,\mathcal{A}^{pp}(s,t)\\ &= -\mathrm{Re}[\mathcal{A}^{pp}(s,t)] + i\,\mathrm{Im}[\mathcal{A}^{pp}(s,t)],\end{aligned} \tag{45}$$

where the phase $\Phi(s,t)$ is given by

$$\Phi(s,t) = 2\pi c_1 - i\,\ln\left(\frac{i\mathrm{Im}[\mathcal{A}^{pp}(s,t)] - \mathrm{Re}[\mathcal{A}^{pp}(s,t)]}{i\mathrm{Im}[\mathcal{A}^{pp}(s,t)] + \mathrm{Re}[\mathcal{A}^{pp}(s,t)]}\right), \tag{46}$$

where $c_1 \in \mathbb{Z}$ is an arbitrary constant that is proportional to the initial values of the amplitude. We note that the factor $e^{\Phi(s,t)}$ changes the relative sign of the real part of the amplitude in Eq. (36). The numerical results of the real and imaginary parts of the modified amplitude, $\tilde{\mathcal{A}}^{pp}$ given in Eq. (45) and the ρ parameter are depicted in Fig. 3. As a result, the real and imaginary parts start from positive and the real part changes the relative sign before the imaginary part for both $\sqrt{s} = 7$ and 13 TeV as shown in Fig. 3(a). Furthermore, the ρ parameter for $\sqrt{s} = 7$ and 13 TeV start

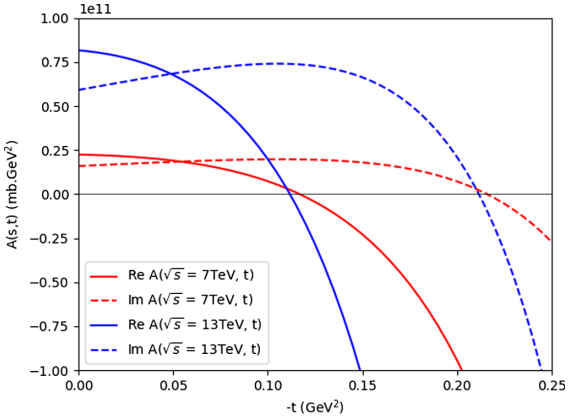

(a) Numerical plots of the real (solid line) and imaginary (dashed line) parts pf the modified amplitude, $\tilde{\mathcal{A}}^{pp}(s,t)$ in Eq.(45) for $\sqrt{s} = 7$ TeV (red) and 13 TeV (blue).

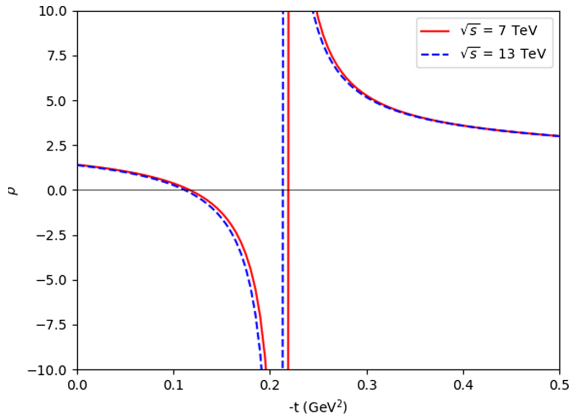

(b) The numerical results of the rho parameter for $\sqrt{s} = 7$ TeV (red solid line) and 13 TeV (blue dashed line) are plotted with respect to $-t$.

FIG. 3. In the left panel, the real part starts from positive and falls to zero before the imaginary part, which satisfies the geometric scaling from Martin's assumption for low $-t$ region. In the right panel, the plots of the ρ parameter for $\sqrt{s} = 7$ and 13 TeV have similar shapes and are qualitatively compatible with the analysis done in Ref. [102].

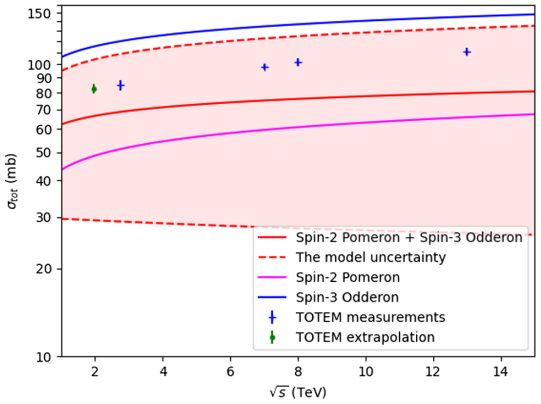

(a) The red line represents the total cross-section, which is the sum of the spin-2 pomeron and the spin-3 odderon. The purple line shows the contribution from the spin-2 Pomeron, and the blue line represents the contribution from the spin-3 odderon.

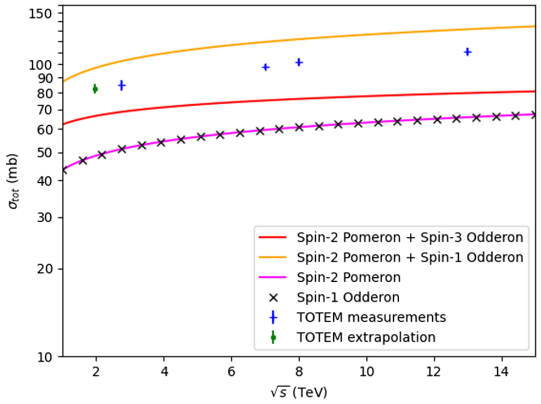

(b) The plots aim to compare our model's predictions with the spin-2 pomeron and spin-1 odderon models constructed in Ref.[48]. As shown in the literature, using the same parameter values for pomeron and odderon, their separate contributions are identical.

FIG. 4. The left panel plot in Eq. (37) shows the total cross section of the pp scattering with exchanges of pomeron spin-2 and odderon spin-3 and the separate contribution to the total cross section from the spin-2 pomeron and the spin-3 odderon. We used the averaged fitted parameters from the combined data set in Table I, and our model is in agreement with the TOTEM pp results at the TeV region. Our model also matches the extrapolation of the TOTEM data at 1.96 TeV for the pp scattering, and all data points are within the prediction band of our model. Additionally, we compared our model with the one in Ref. [48] on the right panel, and we found that the total cross section from the average values of the fitted parameters in our model is lower than the data, whereas the spin-2 pomeron and spin-1 odderon are higher than the data. See the main text for further discussion.

from the positive and change the relative sign to the negative around $-t \approx 0.12$ GeV^2. Interestingly, our results correspond to conclusion of Ref. [102] that the real part of the nuclear amplitude equal to zero at $-t \approx 0.12$ GeV^2. In order to reproduce the experimental data from the ρ parameter at 13 TeV given by LHC [101], our model requires a more detailed modification of the amplitude. However, we have postponed this task to future work.

We close this section by considering the total cross section of the pp in our model. The relevant parameters from the combined dataset are substituted to the total cross section formula in Eq. (37). Then, we plot the total cross section as a function of center of mass energy ($\sqrt{s}$) as shown in Fig. 4(a) and we found that our model of the odderon as Regge oddball spin-3 is compatible with the TOTEM data for pp scattering at the TeV regime. In particular, the extrapolation of TOTEM data for the pp total cross section at 1.96 TeV is also laid within the error band of our model. It should be noted that the large error band in the predicted total cross section is due to the uncertainty of the parameter $\epsilon_{\mathbb{O}}$. This parameter appears as the power of the center of mass energy square, s, in Eq. (37), and its uncertainty is approximately 20%, as shown in Table I. We have also separated the contributions of the pure spin-2 pomeron and spin-3 odderon for the total cross section in Fig. 4(a). Furthermore, it is worth comparing our model's prediction of the total cross section to that of the model in Ref. [48], which utilized $g_{\mathbb{P}} = g_{\mathbb{O}} = 3 \times 1.78$ GeV^{-1}, $\alpha_{\mathbb{P}} = \alpha_{\mathbb{O}} = 0.25$ GeV^{-2} and $\epsilon_{\mathbb{P}} = \epsilon_{\mathbb{O}} = 0.0808$. In Fig. 4(b), we found that our spin-3 odderon and spin-1 odderon model Ref. [48] are qualitatively indistinguishable when compared to the experimental data of the pp total cross section. This means the spin average observable cannot determine which model is better. However, it is possible to differentiate between the contribution of spin-3 odderon and spin-1 odderon using the helicity amplitude formalism. Using the best fit parameters $\epsilon_{\mathbb{P}} = 0.0808$ and $\epsilon_{\mathbb{O}} = 0.0620$, in addition, the total cross section of the present work in Eq. (37) has been checked numerically and it also corresponds to a Froissart bound, i.e., $\sigma_{\text{tot}}^{pp} \leq (\ln s)^2$ at $s \to \infty$ limit.

IV. CONCLUSIONS

In this work, we considered the odderon as the Regge oddball spin-3. The existence of odderon can be observed in a study of the difference between pp and $p\bar{p}$ elastic scattering. We, therefore, investigate pp and $p\bar{p}$ scattering at the Regge limit by including the pomeron and odderon exchanges in the present work. The effective Lagrangians of the processes are constructed and the standard perturbative QFT method is used to calculate the relevant observables in this work. The pomeron and odderon are identified as the Regge tensor glueballs and oddballs with spin-2 and -3, respectively. We have employed the Donnachie-Landschoff ansatz for the pomeron propagator and the Regge trajectory with the electromagnetic type of the pomeron-pp form factor. Furthermore, we also modified the electromagnetic

type of the odderon-pp by introducing three additional free parameters. There are six free parameters of the model in this work $(g_{\mathbb{O}}, \epsilon_{\mathbb{O}}, \alpha'_{\mathbb{O}}, A, B, C)$. Having performed a careful statistical analysis, all free parameters have been fixed by fitting with all combined data of the pp and $p\bar{p}$ differential cross sections at the TeV regime see results in Table I. After fixing the free parameters in the present work, the masses of the odderon spin-3 and their excited states for spin-5 and -7 are estimated from its Regge trajectory by using the best fit of the combined data set. Considering the best-fit results in Table I, the oddereon Regge trajectory parameters are found to be $\alpha'_{\mathbb{O}} = 0.189 \pm 0.038$ and $\epsilon_{\mathbb{O}} = 0.062 \pm 0.011$. These results are compatible with the assumptions in Ref. [48] that used to estimate those two parameters as $\alpha'_{\mathbb{O}} \approx \alpha'_{\mathbb{P}}$ and $\epsilon_{\mathbb{O}} \leq \epsilon_{\mathbb{P}}$. As a result, we found that the tensor odderon masses are heavier than the phenomenological approach by using the double pole Regge model extracted from the experimental data [52]. On the other hand, the odderon masses in this work are lighter than other theoretical model calculations in the literature for all odderons along their trajectory by about 0.3 GeV. In addition, the geometric scaling in Coulomb-nuclear interference region can be demonstrated by applying the phase rotation to the amplitude of our model. Having used the best-fit parameters, the total cross sections also agree with the TOTEM data in the TeV regime and its extrapolation from D0 of the pp scattering at 1.96 TeV. The odderon spin-3 contribution also provided the amplitude in Regge limit that satisfied the Froissart bound. However, we compare the spin-3 odderon model and the spin-1 odderon model in the literature and showed that both models are equally likely to explain the total cross section data. The helicity amplitude could be a good framework to distinguish those two models. According to our findings in this work, the tensor Regge oddball spin-3 particle is a plausible candidate for the odderon. Further studies to confirm our conclusion are needed to investigate other scattering processes such as polarized proton-proton scattering and photoproduction process. We plan to do this in the forthcoming work.

ACKNOWLEDGMENTS

We thank the referee for the helpful comments and suggestions to improve this work. D. S. is supported by the Fundamental Fund of Khon Kaen University and D. S. has received funding support from the National Science, Research and Innovation Fund. The Mindanao State University—Iligan Institute of Technology is also acknowledged through its research and extension support extended to J. B. Magallanes for his travel to Khon Kaen University, Thailand. P. S., C. P., and D. S. are financially supported by the National Astronomical Research Institute of Thailand (NARIT). C. P. and D. S. are supported by Thailand NSRF via PMU-B (Grant No. B37G660013). C. P. is also supported by Fundamental Fund 2565 of Khon Kaen University and Research Grant for New Scholar, Office of the Permanent Secretary, Ministry of Higher Education, Science, Research and Innovation under Contract No. RGNS 64-043. The authors acknowledge the National Science and Technology Development Agency, National e-Science Infrastructure Consortium, Chulalongkorn University and the Chulalongkorn Academic Advancement into Its 2nd Century Project, NSRF via the Program Management Unit for Human Resources & Institutional Development, Research and Innovation (Grants No. B05F650021 and No. B37G660013] (Thailand) for providing computing infrastructure that has contributed to the research results reported within this paper [105].

APPENDIX: ERROR ANALYSIS

We provide the detail of the error estimation method in this section. The errors for parameter fitting in this analysis are handling outside the IMINUIT package due to inaccuracy of the results. The errors shown in Table I are therefore improved by the following. Consider the Taylor expansion around the minimum of the χ^2 function,

$$\chi^2(\alpha_i) \approx \chi^2(\alpha_i^{\min}) + \frac{1}{2}(\alpha_i - \alpha_i^{\min})^2 \left.\frac{\partial \chi^2}{\partial \alpha_i}\right|_{\alpha_i = \alpha_i^{\min}} + \mathcal{O}((\alpha_i - \alpha_i^{\min})^3). \tag{A1}$$

We can approximate the error of parameter estimation, σ_i, using the width of parabolic function defined as

$$\frac{1}{\sigma_i^2} = \frac{1}{2}\left.\frac{\partial \chi^2}{\partial \alpha_i}\right|_{\alpha_i = \alpha_i^{\min}}, \tag{A2}$$

which is also the diagonal component of the Hessian matrix. The second derivative of the χ^2 function is obtained via the finite difference method

$$\left.\frac{\partial \chi^2}{\partial \alpha_i}\right|_{\alpha_i = \alpha_i^{\min}} \approx \frac{\chi^2(a_i^{\min} + \Delta a_i) + \chi^2(a_i^{\min} - \Delta a_i) - 2\chi^2(a_i^{\min})}{\Delta a_i^2}, \tag{A3}$$

where Δa_i is chosen to be sufficiently small compared to the value of the error. The validity of the approximation is then confirmed by the comparison between the parabolic functions and the real χ^2 function shown in Fig. 5. One can see that both functions agree very well within the range of error estimations.

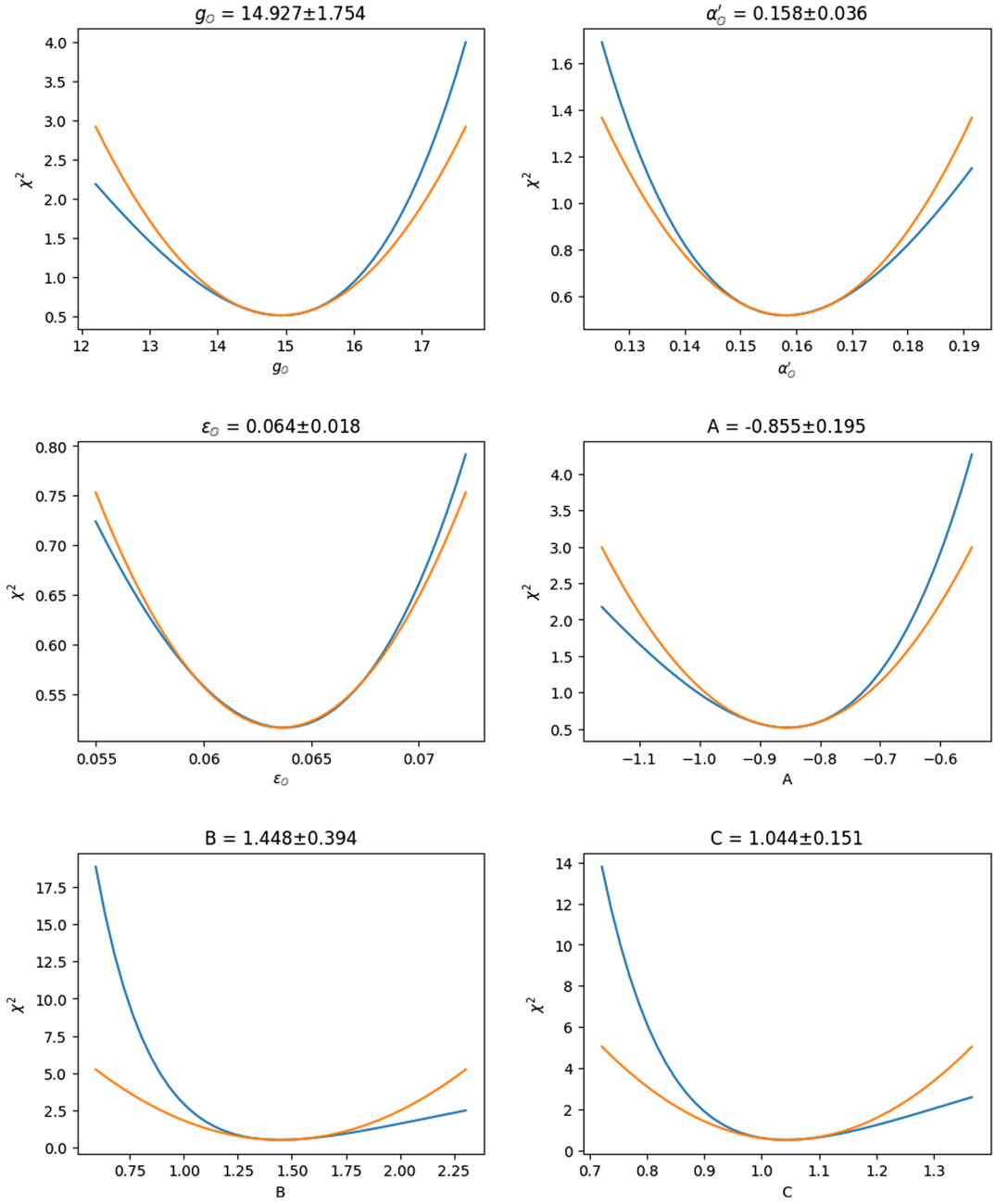

FIG. 5. The comparison plots between the parabolic function using $\chi^2 = \chi^{\min} + \frac{(\alpha_i - \alpha_i^{\min})^2}{\sigma_i^2}$ (orange line) and the real χ^2 function (blue line). The combined dataset of 1.96 GeV (pp, $p\bar{p}$) is used to obtain the parameter fit in these plots. Each panel represents the variation of the χ^2 function in each particular direction of the parameter space.

[1] R. J. Eden, P. V. Landshoff, D. I. Olive, and J. C. Polkinghorne, *The Analytic S-Matrix* (Cambridge University Press, Cambridge, England, 1966).

[2] V. N. Gribov, *The Theory of Complex Angular Momenta: Gribov Lectures on Theoretical Physics*, Cambridge Monographs on Mathematical Physics (Cambridge University Press, Cambridge, England, 2007).

[3] P. D. B. Collins, *An Introduction to Regge Theory and High-Energy Physics*, Cambridge Monographs on Mathematical Physics (Cambridge University Press, Cambridge, UK, 2009).

[4] R. J. Eden, Rep. Prog. Phys. **34**, 995 (1971).

[5] P. D. B. Collins, Phys. Rep. **1**, 103 (1971).

[6] C. B. Chiu, Annu. Rev. Nucl. Part. Sci. **22**, 255 (1972).

[7] A. C. Irving and R. P. Worden, Phys. Rep. **34**, 117 (1977).
[8] G. F. Chew and S. C. Frautschi, Phys. Rev. Lett. **7**, 394 (1961).
[9] V. N. Gribov, JETP Lett. **41**, 667 (1961).
[10] S. Donnachie, H. G. Dosch, O. Nachtmann, and P. Landshoff, *Pomeron Physics and QCD* (Cambridge University Press, Cambridge, England, 2004), Vol. 19.
[11] J. R. Forshaw and D. A. Ross, *Quantum Chromodynamics and the Pomeron*, Cambridge Lecture Notes in Physics Vol. 9 (Cambridge University Press, Cambridge, England, 2022).
[12] P. D. B. Collins, F. D. Gault, and A. D. Martin, Nucl. Phys. **B80**, 135 (1974).
[13] A. Donnachie and P. V. Landshoff, Nucl. Phys. **B244**, 322 (1984).
[14] A. Donnachie and P. V. Landshoff, Phys. Lett. B **296**, 227 (1992).
[15] L. Lukaszuk and B. Nicolescu, Lett. Nuovo Cimento **8**, 405 (1973).
[16] S. V. Akkelin and E. S. Martynov, Sov. J. Nucl. Phys. **53**, 1007 (1991).
[17] E. A. Kuraev, L. N. Lipatov, and V. S. Fadin, Sov. Phys. JETP **45**, 199 (1977).
[18] I. I. Balitsky and L. N. Lipatov, Sov. J. Nucl. Phys. **28**, 822 (1978).
[19] E. A. Kuraev, L. N. Lipatov, and V. S. Fadin, Sov. Phys. JETP **44**, 443 (1976).
[20] L. N. Lipatov, Phys. Lett. B **251**, 284 (1990).
[21] S. Narison, Z. Phys. C **26**, 209 (1984).
[22] S. Narison, Nucl. Phys. **B509**, 312 (1998).
[23] L. Tang and C.-F. Qiao, Nucl. Phys. **B904**, 282 (2016).
[24] H. B. Meyer and M. J. Teper, Phys. Lett. B **605**, 344 (2005).
[25] C. J. Morningstar and M. J. Peardon, Phys. Rev. D **60**, 034509 (1999).
[26] W. Ochs, J. Phys. G **40**, 043001 (2013).
[27] S. R. Cotanch, I. J. General, and P. Wang, Eur. Phys. J. A **31**, 656 (2007).
[28] A. B. Kaidalov and Y. A. Simonov, Phys. Lett. B **636**, 101 (2006).
[29] A. B. Kaidalov and Y. A. Simonov, Phys. Lett. B **477**, 163 (2000).
[30] A. B. Kaidalov and Y. A. Simonov, Phys. At. Nucl. **63**, 1428 (2000).
[31] F. J. Llanes-Estrada, S. R. Cotanch, P. J. de A. Bicudo, J. E. F. T. Ribeiro, and A. P. Szczepaniak, Nucl. Phys. **A710**, 45 (2002).
[32] R. C. Brower, J. Polchinski, M. J. Strassler, and C.-I. Tan, J. High Energy Phys. 12 (2007) 005.
[33] R. C. Brower, M. Djuric, and C.-I. Tan, J. High Energy Phys. 07 (2009) 063.
[34] H. Boschi-Filho and N. R. F. Braga, Eur. Phys. J. C **32**, 529 (2004).
[35] H. Boschi-Filho, N. R. F. Braga, and H. L. Carrion, Phys. Rev. D **73**, 047901 (2006).
[36] P. Colangelo, F. De Fazio, F. Jugeau, and S. Nicotri, Phys. Lett. B **652**, 73 (2007).
[37] D. Li and M. Huang, J. High Energy Phys. 11 (2013) 088.
[38] R. C. Brower, M. S. Costa, M. Djurić, T. Raben, and C.-I. Tan, J. High Energy Phys. 02 (2015) 104.
[39] A. Ballon-Bayona, R. Carcassés Quevedo, M. S. Costa, and M. Djurić, Phys. Rev. D **93**, 035005 (2016).
[40] E. Folco Capossoli and H. Boschi-Filho, Phys. Lett. B **753**, 419 (2016).
[41] E. Folco Capossoli, D. Li, and H. Boschi-Filho, Phys. Lett. B **760**, 101 (2016).
[42] A. Dymarsky and D. Melnikov, J. High Energy Phys. 11 (2022) 164.
[43] H. B. Meyer, D.Phil. Thesis, University of Oxford, 2004.
[44] E. Gregory, A. Irving, B. Lucini, C. McNeile, A. Rago, C. Richards, and E. Rinaldi, J. High Energy Phys. 10 (2012) 170.
[45] Y. Chen *et al.*, Phys. Rev. D **73**, 014516 (2006).
[46] F. J. Llanes-Estrada, P. Bicudo, and S. R. Cotanch, Phys. Rev. Lett. **96**, 081601 (2006).
[47] V. Mathieu, N. Kochelev, and V. Vento, Int. J. Mod. Phys. E **18**, 1 (2009).
[48] C. Ewerz, M. Maniatis, and O. Nachtmann, Ann. Phys. (Amsterdam) **342**, 31 (2014).
[49] C. Ewerz, P. Lebiedowicz, O. Nachtmann, and A. Szczurek, Phys. Lett. B **763**, 382 (2016).
[50] R. J. M. Covolan, J. Montanha, and K. A. Goulianos, Phys. Lett. B **389**, 176 (1996).
[51] M. M. Block and F. Halzen, Phys. Rev. D **86**, 051504 (2012).
[52] I. Szanyi, L. Jenkovszky, R. Schicker, and V. Svintozelskyi, Nucl. Phys. **A998**, 121728 (2020).
[53] L. Jenkovszky, Symmetry **12**, 1784 (2020).
[54] W. Broniowski, L. Jenkovszky, E. Ruiz Arriola, and I. Szanyi, Phys. Rev. D **98**, 074012 (2018).
[55] T. Csorgo and I. Szanyi, Eur. Phys. J. C **81**, 611 (2021).
[56] T. Csörgő, T. Novak, R. Pasechnik, A. Ster, and I. Szanyi, Eur. Phys. J. C **81**, 180 (2021).
[57] T. Csörgő, R. Pasechnik, and A. Ster, Eur. Phys. J. C **79**, 62 (2019).
[58] A. Ster, L. Jenkovszky, and T. Csorgo, Phys. Rev. D **91**, 074018 (2015).
[59] M. M. Block and R. N. Cahn, Rev. Mod. Phys. **57**, 563 (1985).
[60] V. A. Khoze, A. D. Martin, and M. G. Ryskin, Phys. Lett. B **780**, 352 (2018).
[61] F. Halzen, G. I. Krein, and A. A. Natale, Phys. Rev. D **47**, 295 (1993).
[62] A. Donnachie and P. V. Landshoff, Phys. Lett. **123B**, 345 (1983).
[63] W.-X. Ma, A. W. Thomas, P.-N. Shen, and L.-J. Zhou, Commun. Theor. Phys. **36**, 577 (2001).
[64] Z.-H. Hu, L.-J. Zhou, W.-X. Ma, J. Zhang, and J.-F. Liu, Commun. Theor. Phys. **38**, 65 (2002).
[65] X.-R. He, L.-J. Zhou, and W.-X. Ma, Commun. Theor. Phys. **39**, 78 (2003).
[66] Z.-H. Hu, L.-J. Zhou, and W.-X. Ma, Commun. Theor. Phys. **49**, 729 (2008).
[67] L.-J. Zhou, Z.-H. Hu, and W.-X. Ma, Commun. Theor. Phys. **45**, 1069 (2006).
[68] J. Lu, L.-J. Zhou, and Z.-J. Fang, Chin. Phys. C **44**, 024105 (2020).
[69] J. Bartels, L. N. Lipatov, and G. P. Vacca, Phys. Lett. B **477**, 178 (2000).

[70] S. K. Domokos, J. A. Harvey, and N. Mann, Phys. Rev. D **80**, 126015 (2009).
[71] S. K. Domokos, J. A. Harvey, and N. Mann, Phys. Rev. D **82**, 106007 (2010).
[72] E. Avsar, Y. Hatta, and T. Matsuo, J. High Energy Phys. 03 (2010) 037.
[73] Z. Hu, B. Maddock, and N. Mann, J. High Energy Phys. 08 (2018) 093.
[74] W. Xie, A. Watanabe, and M. Huang, J. High Energy Phys. 10 (2019) 053.
[75] P. Burikham and D. Samart, Eur. Phys. J. C **79**, 452 (2019).
[76] Z. Liu, W. Xie, and A. Watanabe, Phys. Rev. D **107**, 014018 (2023).
[77] Z. Liu, W. Xie, F. Sun, S. Li, and A. Watanabe, Phys. Rev. D **106**, 054025 (2022).
[78] A. Ballon-Bayona, R. Carcassés Quevedo, and M. S. Costa, J. High Energy Phys. 08 (2017) 085.
[79] I. Iatrakis, A. Ramamurti, and E. Shuryak, Phys. Rev. D **94**, 045005 (2016).
[80] V. M. Abazov *et al.* (D0 Collaboration), Phys. Rev. D **86**, 012009 (2012).
[81] V. M. Abazov *et al.* (TOTEM, D0 Collaborations), Phys. Rev. Lett. **127**, 062003 (2021).
[82] H.-X. Chen, W. Chen, and S.-L. Zhu, Phys. Rev. D **104**, 094050 (2021).
[83] H.-X. Chen, W. Chen, and S.-L. Zhu, Phys. Rev. D **103**, L091503 (2021).
[84] L. Zhang, C. Chen, Y. Chen, and M. Huang, Phys. Rev. D **105**, 026020 (2022).
[85] N. Bence, A. Lengyel, Z. Tarics, E. Martynov, and G. Tersimonov, Eur. Phys. J. A **57**, 265 (2021).
[86] E. F. Capossoli, J. P. M. Graça, and H. Boschi-Filho, Phys. Rev. D **105**, 026026 (2022).
[87] P. Lebiedowicz, SciPost Phys. Proc. **6**, 010 (2022).
[88] C. Baldenegro, C. Royon, and A. M. Stasto, Phys. Lett. B **830**, 137141 (2022).
[89] Z.-F. Cui, D. Binosi, C. D. Roberts, S. M. Schmidt, and D. N. Triantafyllopoulos, Phys. Lett. B **839**, 137826 (2023).
[90] P. Lebiedowicz, O. Nachtmann, and A. Szczurek, Phys. Rev. D **106**, 034023 (2022).
[91] C. Bonanno, M. D'Elia, B. Lucini, and D. Vadacchino, Proc. Sci. LATTICE2022 (**2023**) 392.
[92] M. E. Peskin and D. V. Schroeder, *An Introduction to Quantum Field Theory* (Addison-Wesley, Reading, USA, 1995).
[93] F. Close, S. Donnachie, and G. Shaw, eds., *Electromagnetic Interactions and Hadronic Structure* (Cambridge University Press, Cambridge, England, 2009), Vol. 25.
[94] F. A. Berends and J. C. J. M. van Reisen, Nucl. Phys. **B164**, 286 (1980).
[95] C. Avila *et al.* (E811 Collaboration), Phys. Lett. B **445**, 419 (1999).
[96] G. Antchev *et al.* (TOTEM Collaboration), Eur. Phys. J. C **80**, 91 (2020).
[97] G. Antchev *et al.* (TOTEM Collaboration), Europhys. Lett. **101**, 21002 (2013).
[98] G. Antchev *et al.* (TOTEM Collaboration), Eur. Phys. J. C **79**, 103 (2019).
[99] H. Dembinski *et al.* (2020), 10.5281/zenodo.3949207.
[100] F. James and M. Roos, Comput. Phys. Commun. **10**, 343 (1975).
[101] G. Antchev *et al.* (TOTEM Collaboration), Eur. Phys. J. C **79**, 785 (2019).
[102] G. Pancheri, S. Pacetti, and Y. Srivastava, Phys. Rev. D **99**, 034014 (2019).
[103] A. Martin, Lett. Nuovo Cimento **7**, 811 (1973).
[104] A. Martin, Phys. Lett. B **404**, 137 (1997).
[105] www.e-science.in.th.